Supporting Information

Nanostrip Flexible Microwave Enzymatic Biosensor for Noninvasive Epidermal Glucose Sensing

*Qiannan Xue[#], Zheyu Li[#], Qikun Wang, Wenwei Pan, Ye Chang, Xuexin Duan**

Q. Xue, Z. Li, Q. Wang, W. Pan, Y. Chang, Prof. X. Duan
State Key Laboratory of Precision Measuring Technology & Instruments, School of Precision Instruments and Optoelec-tronics Engineering, Tianjin University, Tianjin 300072, China
E-mail: xduan@tju.edu.cn

Keywords: glucose detection, microstrip antenna, microwave sensor, nanowire, wearable sensor

S1. Design of the nanostrips antennas

The local electric field of microstrip and nanostrip attena is simlulted in Figure S1a. The nanostrip presents a clear microwave enhancement with the conventional microstripe antenna. Here, we discussed furtherly on the geometry effects (size, distribution, and the density) of the nanostrips. The microwave enhacement by the nanostrips is mainly due to the fact that the nanoscale line width of the nanostrip increases the local current density and ultimately leads to an increase in the electric field strength. Such size effect can be explained by *eq s1*[1, 2]:

$$\sigma_e = E_0 \varepsilon_p \sim \frac{1}{r} \qquad (s1)$$

where σ_e is the surface charge density, E_0 is the electric field intensity, r is the radius of curvature of the stripline, and ε_p is dielectric constant of the attena strip. It clearly shows that the surface charge density is reversily propotional to the radius of curvature of the stripline. Thus, reducing the width of the stripline can induce stronger electric field intensity of the microwave.

The simualtion result of the electric field distribution of the sensors based on disordered nanostrips is shown in Figure S1b. The reflection coefficient magnitude of the microwave antennas with the same nanostrips but disordered shows very weak signal.

Next, the density effect of the nanowires is further discussed. The electric field distribution (Figure S1c) and peak reflection coefficient (Figure S1d) of 0, 5 ,30, 50 nanowires (corrspoding to the distance between the neighboured nanowires 0μm, 500 μm, 86 μm, 50 μm on the same microwave sensor at 2.24 GHz were simulated. It shows that the electric field strength and the microwave signal increase with the number of nanowires per sensor surface unit. This can be explained by *eq s2*[3]:

$$E_a = V/(1/2)^{1/2} d\, \varepsilon_{inter} \qquad (s2)$$

where, E_a is the average electric field strength, V is the applied voltage, d and ε_{inter} are the diatance and the permittivity between the neighboured nanowires. It shows that the average electric field strength varies inversely with the distance of the nanowires, d. Smaller distance

between the neighboured nanowires (higher density) will result stronger interface polarization, leading to a larger GHz absorption peak. This is also consistent with the previously published result, where it shows that the maximum absorption peak is enhanced with increasing of the number of the nanowires[4].

Though the theory analysis indicates narrower nanowires, higher density of the nanowires are preferred to achieve the maximum microwave enhancement effect, we still need to consider the limitation of the materials and fabrication cost of the nanowires. In this work, to facilitate the solution process and glucose sensing, biotin doped PEDOT: PSS is used as the material of the stripeline. The typical size of PEDOT: PSS nanoparticle domain is about 60 nm[5], the line width of 100 nm ensures that the PEDOT:PSS can form continuous 1D nanowires without clogging. Regarding the density, as the nanowires are fabricated by the nanoscale soft printing approach, the distance between the neighbored nanowires is based on the nanomold. Higher density of the nanowires will increase the cost of the nanomold. Besides, if the space between the neighbored nanowires is too short, it cannot achieve good conformal contact between the PDMS mold and the substrate, which will result leaking of the PEDOT:PSS solution during the capillary filling and significantly reduce the quantity of the nanowires. Considering the intensity of the absorption peak did not change too much in the range of sub-10 micrometer space between the neighbored nanowires (Figure S1e&f), we used the averaged 4 μm spacing in this work.

Overall, the designed template contains parallel nanogrooves with a cross section of 100 nm (width) × 60 nm (depth) and the spacing between the neighbored nanogroove is 3 μm and 5 μm

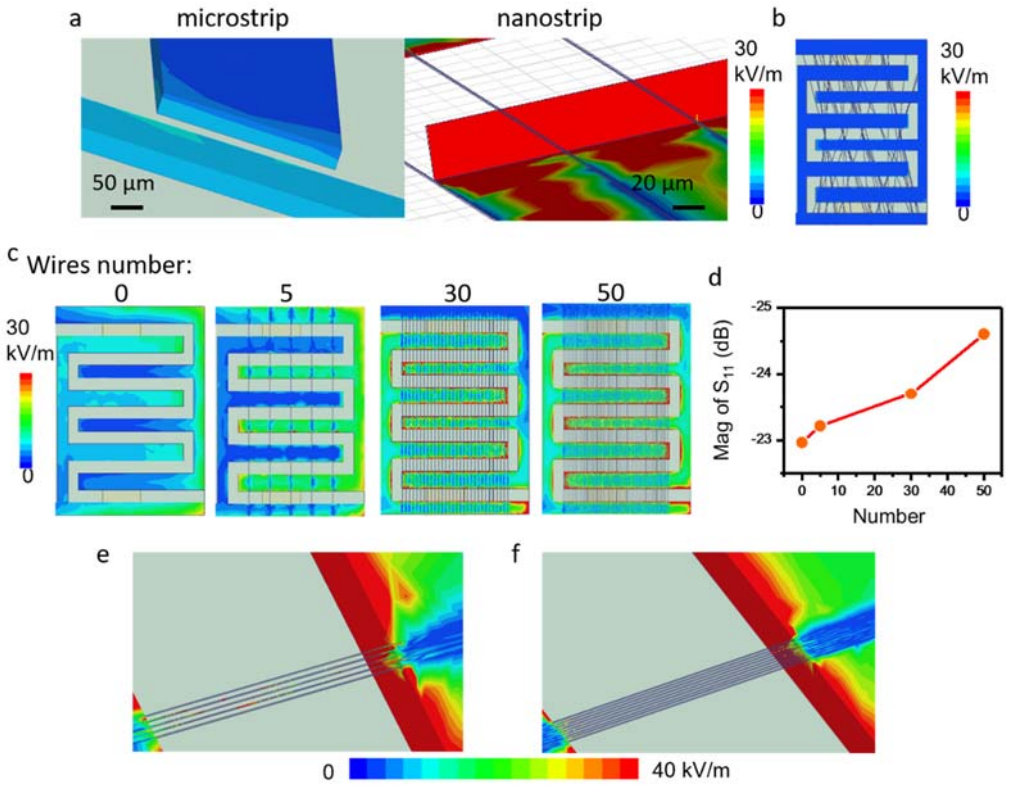

Figure S1. Local electric field of microstrip and nanostrip a); electric field distribution of the proposed sensor with disordered nanostrips b); electric field distribution varies with the increased of the numbers of the nanowires c); magnitude of reflection coefficient simulation with the nanowires number d); electric field distribution of line spacing of 4µm e) and 2µm f).

S2. Characterizations of the nanowires array

The nanostrip sensor consists of nanowires array, which is prepared based on nanoscale printing technology. Figure S2 shows the chemical stucture of the inks (PEDOT:PSS dopted with PEGylated biotin-derivatized polyelectrolytes).

Figure S3a&b show the optical microscopy and laser confocal microscopy images of the printed nanowires array on the polyethylene terephthalate substrate. The nanowires are well prepared and distributed in a large area. After metal evaporation, electrical test of the nanowires were condcuted. IV test confirms a good ohmic characteristics and the resistance value is 0.3MΩ, which closely matches the calculated resistance of the nanowires array (Figure S3c).

We used laser confocal microscopy to measure the height changes of nanowires before and after the immobilization of GOx by biotin-streptavidin-biotin conjugation. The average height is increased from 37.5 nm to 54.8 nm (Figure S4).

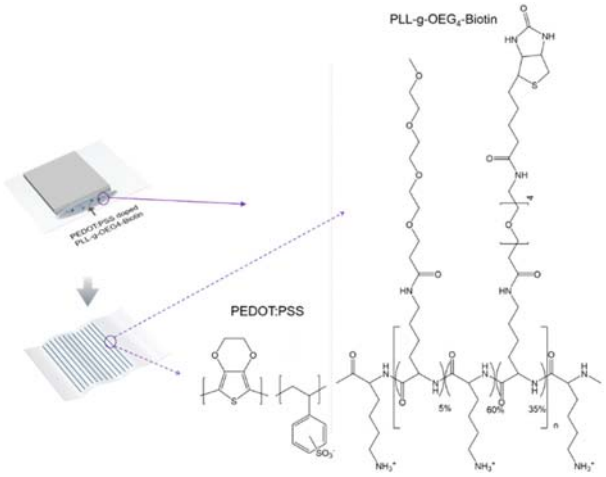

Figure S2. The chemical structure of PEDOT:PSS doped PLL-g-OEG4-Biotin

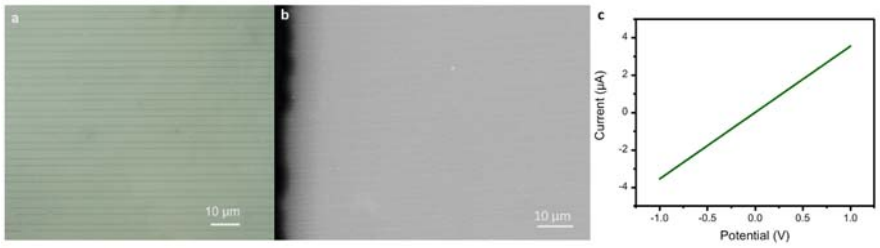

Figure S3. Optical a) and laser confocal microscopy b) images of the nanowires; The electrical characterization of the nanowires c).

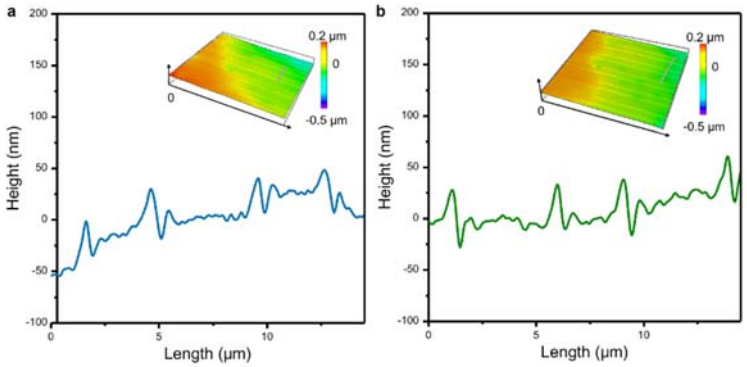

Figure S4. Height changes of nanowire before a) and after b) the immobilization of GOx by biotin-streptavidin-biotin conjugation by laser confocal microscopy

S3. Microwave spectrum of the enzyme immobilization process

After the fabrication of nanostrip microwave sensor, the reflection coefficient before and after the modification of SAv were measured. Then, the reflection coefficient of the microwave sensor was tested after the glucose oxidase was immobilized by SAv-biotin conjunction. Figure S5 shows that the S_{11} magnitude increased in turn after SAv modification and GOx immobilization,.

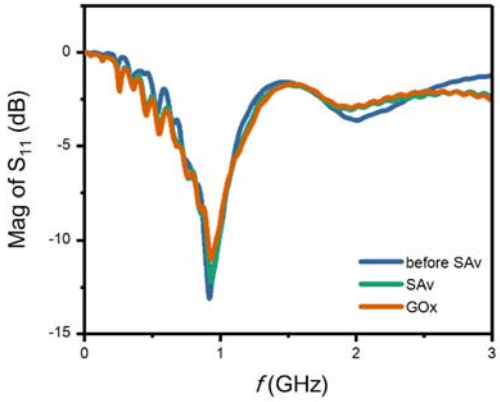

Figure S5. S_{11} magnitude spectra of samples without modification, after SAv binding, and after GOx immobilization.

S4. Stability testing

In the stability test, the sensor worked continuously in 0.1 nM, 10 nM and 10 μM glucose solutions for 10, 50 and 100 mins, respectively. The responses of the long-term tests were recorded, and the differences are 0.25%, 0.67% and 0.43% respectively. The results confirm that the sensor has a rather stable response and a small drift.

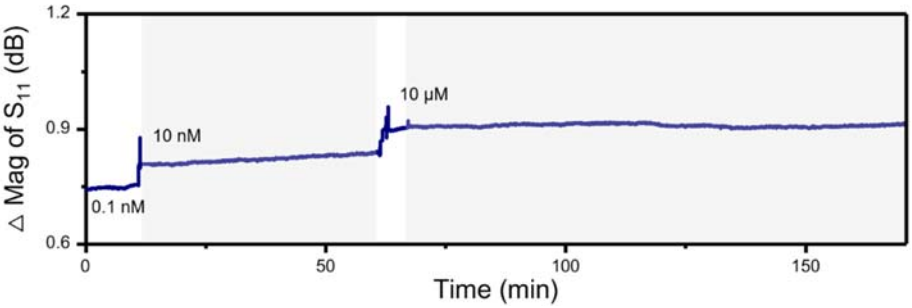

Figure S6. long-term glucose measurement with the proposed microwave biosensor

S5. Kinetics analysis

The response of the sensor conforms to the Lineweaver–Burk equation[6], where R is the response loss of sensor, $[S]$ is the glucose concentration, R_{max} is the maximum of sensor response and k_m is the Michaelis Constant. The fitting curve is shown in Figure S7. The Michaelis Constant of the enzyme fixed by the sensor is calculated as 4.6×10^{-5} mM.

$$\frac{1}{R} = \frac{k_m}{R_{max}} \times \frac{1}{[S]} + \frac{1}{R_{max}} \quad \textbf{(s1)}$$

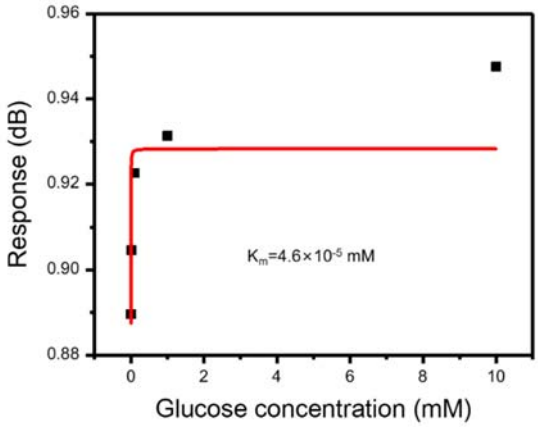

Figure S7. the fitting curve of Lineweaver–Burk equation

S6. Reflection coefficient of film-based microwave biosensor

The mechanism for the glucose detection by the microwave sensor proposed in this paper is that the generation of hydrogen peroxide due to the enzymatic decomposition causes the microwave peak to decay. Therefore, a large initial peak is a prerequisite for the glucose test. According to the simulation results, the initial microwave peak based on the disordered nanostrips is very weak, so it is reasonable to believe that it is not very suitable for the test of this system. Performance of biosensors based on film and ordered nanostrips in glucose solutions is further compared.

The film-based microwave sensor was placed in a 10 nM glucose solution and its reflection coefficient spectrum was collected. The result shows the response amplitude is reduced, compared with nanostrips-based microwave sensors (Figure S8). Although the simulation cannot fully simulate the actual test conditions, the experimental and simulation trends are consistent, which proves that the introduction of nanowires has played a good role in enhancing microwave signals.

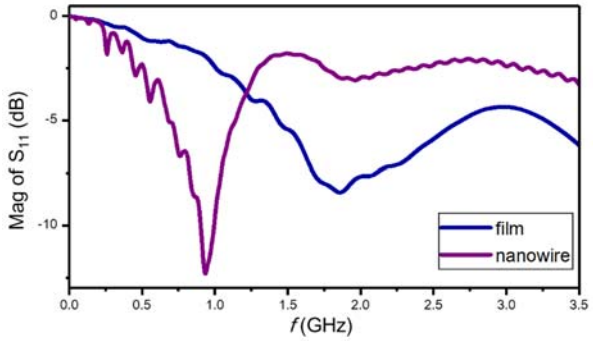

Figure S8. S_{11} magnitude spectra of film-based and nanostrips-based microwave biosensor.

S7 Interference testing

The sensor was placed in several possible interfering substances in sweat, including ultra pure water, 0.5% lactic acid, 0.1% sodium dihydrogen phosphate and 0.1% urea respectively. Meanwile, 50nM of glucose solution is tested. As shown in Figure S9, the response of the sensor to glucose is significantly higher than that of other substances, indicating that the sensor has good selectivity.

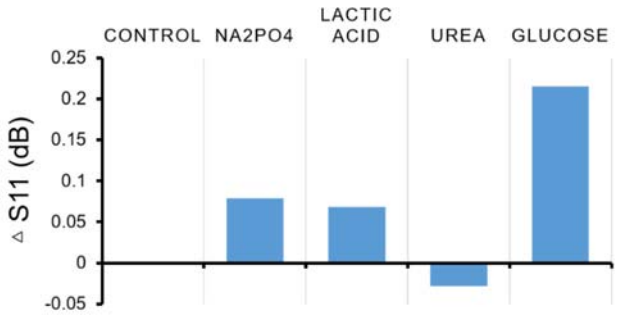

Figure S9. Response comparison of the biosensor in several possible interfering substances in sweat.

S8. Performance comparison of reported nonintrusive glucose biosensor

Compared with the eight kinds of nonintrusive glucose sensors reported recently (Table S1), the microwave biosensor proposed in this paper has a wider detection range, acceptable linearity, and can distinguish lower response concentration.

Table S1. Performance comparison of reported glucose biosensor

method		Detection range	LOD	Linearity	Response time (s)	Is it wearable?
Chronoamperometry	[7]	10μM-500μM	10μM	-	-	Yes
	[8]	50μM-300μM	1.3μM	-	10	Yes
	[9]	0.1mM-1.4mM	5μM	0.99	20	Yes
	[10]	0.05mM-1mM	11μM	0.99	6	Yes
Field effect transistor	[11]	1.5-15mM	1.5mM	0.98	-	No
	[12]	0.5 μM-1 mM	10nM	-	-	Yes
Electrochemical impedance spectroscopy	[13]	0.56μM-11.1mM	5.6μM	0.95	-	Yes
microwave sensor	[14]	0.6-5.6M	0.6M	0.987	-	No
Proposed biosensor		0.1nM-1mM	0.1nM	0.97	4	Yes

S9. Bending test

Under the condition of bending to 36°, the sensor was used to measure the glucose solution with concentration of 0.1nM, 10nM, 1 μM, 10 μM, 100 μM and 1mM in turn, and the peak value of its reflection coefficient spectrum was recorded. As shown in Figure S10& S11, the sensor can distinguish trace amount of glucose and shows good linearity (R^2=0.97), with a minimum distinguishable glucose concentration of 0.1nM.

As shown in Figure S10 and Figure 5a, the characteristic frequencies are different under different bending states. In subsequent practical applications, fast algorithms[15] can be used to determine the degree of bending according to different characteristic frequencies of waveforms and obtain corresponding calibration curves for measurement.

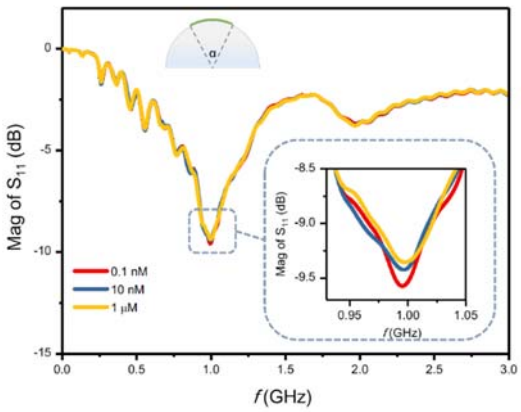

Figure S10. The magnitude of S11 of sensor in bending state for three glucose concentrations detection

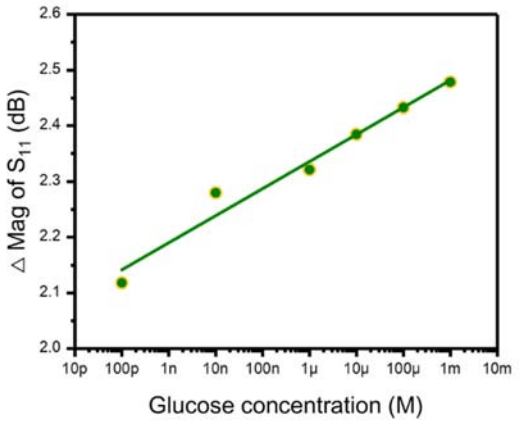

Figure S11. The response of biosensor in bending state vs the glucose solution with different concentration.

S10. Preparation and characterization of PDMS porous membrane

The PDMS membranes was first prepared by spin-coating the liquid prepolymer of the PDMS agent in a 10:1 (w/w) ratio onto a flat glass wafer. After curing, the film thickness (281.8 μm) was determined by confocal laser microscopy (Figure S12a and S12b). Next, a laser beam was pllied to punch holes in the film with a typical diameter of 200 μm and a spacing of 280 μm (Figure S12c). Figure S12d shows a photo of the test system. After the sensor attached to the skin, the microwave spectrum can be collected by the tablet. The input power to the sensor of the miniaturized VNA is 0 dbm (1 mW), which proves that the power consumption of the sensor is very low.

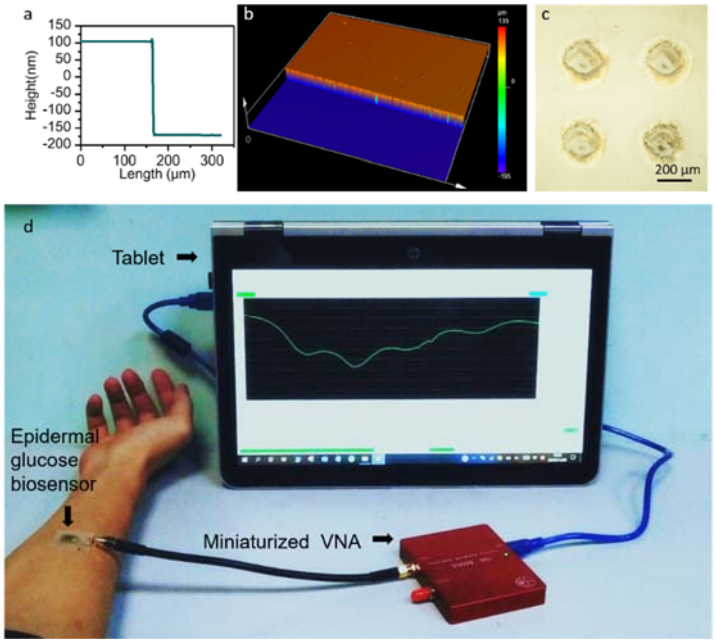

Figure S12. The PDMS film thickness of was measured by laser confocal microscope: 3D view a) and height information b); Optical micrograph of PDMS porous film c); photo of glucose epidermal sensing using a miniaturized vector network (VNA) device and a tablet with wave analysis software d).

References

1. N. Gauthier, *Physics Education*, 1990, **25**, 7-7.
2. L. Enze, *J. Phys. D: Appl. Phys.*, 1986, **19**, 1-6.
3. N. Ranjan, M. Mertig, G. Cuniberti and W. Pompe, *Langmuir*, 2010, **26**, 552-559.
4. Y. Chen, M. Cao, T. Wang and Q. Wan, *Appl. Phys. Lett.*, 2004, **84**, 3367-3369.
5. J. Zhou, D. H. Anjum, L. Chen, X. Xu, I. A. Ventura, L. Jiang and G. Lubineau, *J. Mater. Chem. C*, 2014, **2**, 9903-9910.
6. S. Idris, N. H. Azeman, N. A. Noor Azmy, C. T. Ratnam, M. A. Mahdi and A. A. A. Bakar, *Sens. Actuators, B*, 2018, **273**, 1404-1412.
7. Y. Lin, M. Bariya, H. Y. Y. Nyein, L. Kivimäki, S. Uusitalo, E. Jansson, W. Ji, Z. Yuan, T. Happonen, C. Liedert, J. Hiltunen, Z. Fan and A. Javey, *Adv. Funct. Mater.*, 2019, **29**, 1902521.
8. S. Y. Oh, S. Y. Hong, Y. R. Jeong, J. Yun, H. Park, S. W. Jin, G. Lee, J. H. Oh, H. Lee, S.-S. Lee and J. S. Ha, *ACS Appl. Mater. Interfaces*, 2018, **10**, 13729-13740.
9. X. Xuan, H. S. Yoon and J. Y. Park, *Biosens. Bioelectron.*, 2018, **109**, 75-82.
10. M. Figiela, M. Wysokowski, M. Galinski, T. Jesionowski and I. Stepniak, *Sens. Actuators, B*, 2018, **272**, 296-307.
11. C.-L. Hsu, J.-H. Lin, D.-X. Hsu, S.-H. Wang, S.-Y. Lin and T.-J. Hsueh, *Sens. Actuators, B*, 2017, **238**, 150-159.
12. Q. Liu, Y. Liu, F. Wu, X. Cao, Z. Li, M. Alharbi, A. N. Abbas, M. R. Amer and C. Zhou, *ACS Nano*, 2018, **12**, 1170-1178.
13. R. D. Munje, S. Muthukumar and S. Prasad, *Sens. Actuators, B*, 2017, **238**, 482-490.
14. Z. Abedeen and P. Agarwal, *Sens. Actuators, A*, 2018, **279**, 132-139.
15. F. Boeykens, H. Rogier and L. Vallozzi, *IEEE Transactions on Antennas and Propagation*, 2014, **62**, 1253-1260.